Impurity effects on the melting of Ni clusters

Andrey Lyalin,[1,2,*] Adilah Hussien,[1] Andrey V. Solov'yov,[1,†] and Walter Greiner[1]

[1]*Frankfurt Institute for Advanced Studies, Goethe-University, Ruth-Moufang-Str. 1, 60438 Frankfurt am Main, Germany*

[2]*Imperial College London, Physics Department, Prince Consort Road, London SW7 2BW, UK*

(Dated: August 8, 2008)

We demonstrate that the addition of a single carbon impurity leads to significant changes in the thermodynamic properties of Ni clusters consisting of more than a hundred atoms. The magnitude of the change induced is dependent upon the parameters of the Ni–C interaction. Hence, thermodynamic properties of Ni clusters can be effectively tuned by the addition of an impurity of a particular type. We also show that the presence of a carbon impurity considerably changes the mobility and diffusion of atoms in the Ni cluster at temperatures close to its melting point. The calculated diffusion coefficients of the carbon impurity in the Ni cluster can be used for a reliable estimate of the growth rate of carbon nanotubes.

I. INTRODUCTION

Thermodynamic properties of atomic clusters depend considerably on the cluster size. It has been shown that the melting temperature of a small spherical particle decreases with the reduction of its radius.[1,2,3,4,5] This is due to the substantial increase in the relative number of weakly bounded atoms on the surface in comparison with those in the bulk. Such a size effect on the melting temperature of small particles of different metals having diameters down to 2-3 nm has been confirmed in series of experiments.[6,7,8,9]

However for clusters having sizes smaller than 1-2 nm, the melting temperature is no longer a monotonic function of the cluster size. Experiments on sodium clusters Na_N, with number of atoms $N = 50-360$, have demonstrated that melting temperature as a function of size shows a prominent irregular structure with local maxima.[10,11,12,13] The origin of the non-monotonic variation in the melting temperature with respect to cluster size lies in interplay between electronic and geometric shell effects in the sodium clusters.[13] Intensive theoretical

efforts have been undertaken to identify the details of the geometric and electronic structures underlying the variations in the melting temperature.[14,15,16,17,18,19,20,21]

Experiments on small cluster ions of tin[22] and gallium[23] have confirmed the violation of the linear relationship between the reduction in the melting temperature and the inverse radius of the cluster. It was discovered that the melting temperature of selected Sn_N and Ga_N clusters, of sizes $N < 40$, can considerably exceed the melting temperature of the corresponding bulk material.[22,23] This behavior was explained by the structural differences between the small clusters and the bulk.[22]

Modification of a cluster structure can also be induced by the doping of an impurity or substitution of one or several atoms in a pure cluster with an atom of a different type.[24] It has been shown that doping of sodium clusters with Li, Cs and O_2 impurities (as well as Al_{13} and Ga_{13} clusters with a carbon impurity) results in a decrease of the melting temperature of the cluster.[25,26,27] Whereas doping of the icosahedral silver clusters with Ni and Cu atoms considerably increases the melting temperature.[28] Therefore one can suppose that the thermodynamic properties of a selected cluster can be tuned by doping with an impurity of a particular type.

In this paper we report the results of a systematic theoretical study regarding the effect of impurity on the thermodynamic properties of Ni clusters. We demonstrate that adding a single carbon impurity can result in changes in the melting temperature of an Ni_{147} cluster. The magnitude of the change induced is dependent upon the parameters of the interaction between the Ni atoms and the C impurity. Hence, thermodynamic properties of Ni clusters can be effectively tuned by the addition of an impurity. We also show that the presence of a carbon impurity considerably changes the mobility of atoms in the Ni cluster at temperatures close to its melting point.

The choice of Ni clusters is stipulated by their high chemical and catalytic reactivity, unique properties and multiple applications in nanostructured materials.[29] An important example of such an application is the process of the catalytically activated growth of carbon nanotubes. The mechanism of this process is not yet well understood (see, e.g., Refs. 30, 31,32 and references therein) and knowledge of the specific role of the impurity in the Ni catalytic nanoparticle may ascertain whether the carbon nanotube structure and its growth kinetics can be controlled. The thermodynamic state of the catalytic nanoparticle plays a crucial role on the carbon nanotube growth.[33] The nanotube growth rate can be obtained

by a solution of a set of kinetic equations which include, in particular, the diffusion flux of carbon through the metal particle.[32,34,35] On the other hand the diffusion coefficients depend on the thermodynamic state of the catalytic Ni cluster which can, in turn, be tuned by doping with an impurity. Therefore direct molecular dynamics study of carbon diffusion in the Ni cluster is important for a reliable estimation of the growth rate of carbon nanotubes.

II. THEORETICAL METHODS

The study of structural and dynamical properties of the clusters of transition metals is a challenging task due to the presence of unfilled valence d-orbitals. The high density of the d-states and their localized character make the direct *ab initio* methods computationally very demanding for clusters larger than several dozens of atoms.[36] In order to describe the structure of clusters of larger sizes, one needs to use approximate methods and model interatomic potentials.

An effective approach for study of transition-metal clusters is the embedded-atom method[37,38,39,40,41,42] which takes into account many-body effects. The latter appears through the inhomogeneous electron density of the system. In this paper, the molecular dynamics study of the Ni_{147} cluster has been performed using the Sutton-Chen[37] many-body potential which belongs to the family of the embedded-atom types of potentials. The Sutton-Chen potential has been shown to reproduce bulk and surface properties of transition metals and their alloys with sufficient accuracy (see, e.g., Refs. 36,43,44,45,46 and references therein). The potential energy of the finite system within the Sutton-Chen model has the following form:

$$U_{pot} = \varepsilon \sum_i \left[\frac{1}{2} \sum_{j \neq i} \left(\frac{a}{r_{ij}} \right)^n - c\rho_i^{1/2} \right], \tag{1}$$

where

$$\rho_i = \sum_{j \neq i} \left(\frac{a}{r_{ij}} \right)^m. \tag{2}$$

Here r_{ij} is the distance between atoms i and j, ε is a parameter with dimension of energy, a is the lattice constant, c is a dimensionless parameter, and n and m are positive integers

with $n > m$. The parameters provided by Sutton and Chen for nickel have the following values:[37] $\varepsilon = 1.5707 \cdot 10^{-2}$ eV, $a = 3.52$ Å $c = 39.432$, $n = 9$, and $m = 6$.

The determination of a reliable model potential for the Ni – C interaction is a difficult task. In Refs. 47,48,49 the binding energy and different charge state of various forms of NiC_n clusters (n= 1 - 3) were determined using *ab initio* density functional calculations based on the three-parameter Becke-type gradient-corrected exchange functional with the gradient-corrected correlation functional of Lee, Yang, and Parr (B3LYP)[50,51,52] and LANL2DZ basis set (see, e.g., Ref. 53 and references therein). This was done in order to develop a many-body potential for the transition metal – carbon interaction. The many-body potential was then successfully used for a molecular dynamics study of the formation of metallofullerenes[47] and single-walled carbon nanotubes.[48]

In the present work, however, the interaction between Ni atoms and C impurity is modeled by the Morse pair potential:

$$V^{Ni-C}(r) = \varepsilon_M \left(\left(1 - e^{\rho(1-r/r_0)}\right)^2 - 1 \right). \tag{3}$$

We have determined the parameters of the Morse potential ($\varepsilon_M = 2.431$ eV, $\rho = 3.295$, $r_0 = 1.763$ Å) by fitting the Ni – C interaction obtained in Refs. 47,48,49 within the B3LYP/LANL2DZ method. The choice of using the pairwise Morse potential is due to its simplicity which allows us to study the influence of the parameters in (3) on the thermodynamic properties of the C-doped Ni_{147} clusters, keeping a clear physical picture of the process occuring in the system.

The optimized initial geometries of the cluster have been determined by finding local minima on the multidimensional potential energy surface. We have applied an efficient scheme of global optimization, called the Cluster Fusion Algorithm (CFA).[54,55,56] The CFA belongs to the class of genetic global optimization methods,[57,58] which are very promising for structural optimization of nanoalloys, see, e.g., Ref. 59 and references therein. The scheme has been designed within the context of determination of the most stable cluster geometries and it is applicable for various types of clusters.[54,60,61,62]

Molecular dynamics simulations have been performed for the canonical (NVT) ensemble of particles: the number of particles N, the volume V and the temperature T of the system are kept constant. Integration of Newton's equations of motion have been done using the Verlet leapfrog algorithm, with a time step $\Delta t = 1$ fs and a total simulation run of 10 ns

(excluding an initial equilibration time of 50 ps). For temperature control, we have used the Nosé-Hoover thermostat[63,64] because it correctly generates a canonical ensemble.

III. NUMERICAL RESULTS AND DISCUSSION

During the last, decade numerous theoretical and experimental efforts have been devoted to studying structural, electronic, and magnetic properties of Ni clusters (recent comprehensive reviews can be found in Refs. 65,66). It has been demonstrated that for small Ni clusters, a motif based on the icosahedral structure dominates the cluster growth, at least around sizes of complete Mackay icosahedra.[46,67,68,69] The results of the geometry optimization for the pure and the C-doped Ni_{147} clusters are shown in Fig. 1. The ground state of the Ni_{147} cluster is a perfect icosahedron, Fig. 1(a), in agreement with the results of the previous works (see Refs. 65,69 and references therein).

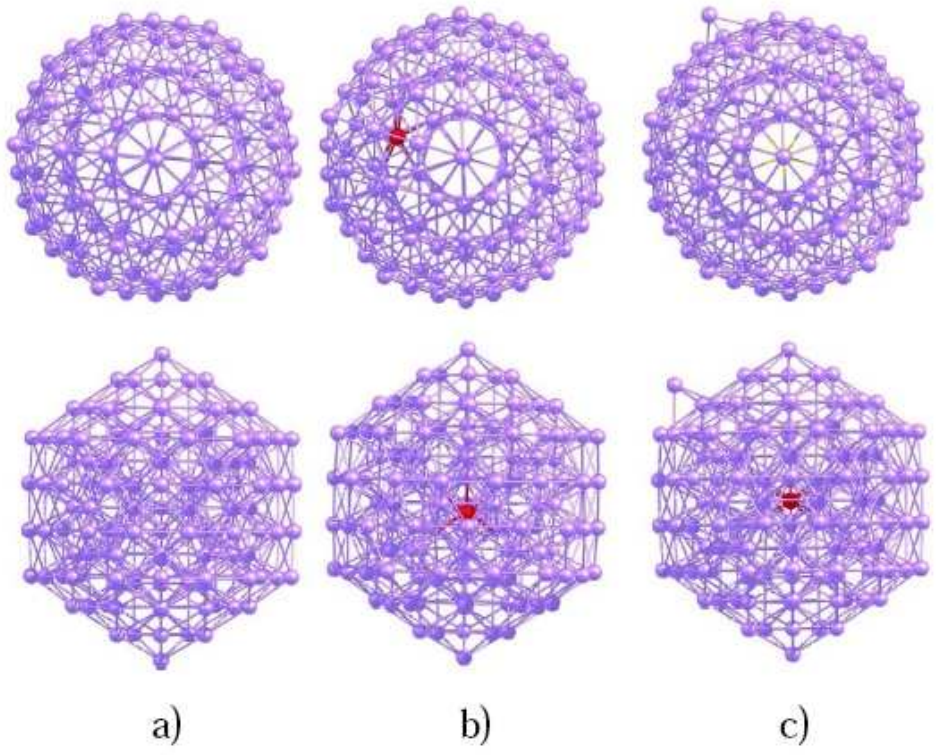

FIG. 1: (Color online) — (a) Optimized structure of a pure Ni_{147} cluster; (b) the *isomer* state structure of the C-doped Ni_{147} cluster; (c) the *ground* state structure of the C-doped Ni_{147} cluster.

For the C-doped Ni_{147} cluster we found that the lowest energy state possesses the icosa-

hedral type of structure with the C atom in the central position and one Ni atom outside the filled icosahedral shell, as shown in Fig. 1(c). The energetically closest isomer of the C-doped Ni_{147} cluster is the deformed icosahedron with the C impurity located in the vicinity of the cluster center, as depicted in Fig. 1(b). The impurity creates a local distortion between the first and the second closed icosahedral shells. The difference in the binding energy per atom between the ground, Fig. 1(c), and the isomer, Fig. 1(b), states of the C-doped Ni_{147} cluster is 0.002 eV. The isomer state, Fig. 1(b), is metastable because in order to transform the cluster structure from the isomer, Fig. 1(b), to its ground state, Fig. 1(c), it is necessary to overcome the energy barrier. The isomer, Fig. 1(b), can be naturally formed by successive migration of the outer C atom from the cluster surface towards its center. Namely, this type of isomer are presumably formed in carbon nanotube growth experiments where a molecule of a feedstock gas or a free C atom collides with the surface of the Ni particle. Therefore, we have performed molecular dynamics simulations for the initial geometry corresponding to the isomer state, Fig. 1(b) of the C-doped Ni_{147} cluster.

A. Pure Ni_{147} clusters

Figures 2 and 3 demonstrate the temperature dependence of the time-averaged total energy $\langle E_{tot} \rangle$ (i.e. the caloric curve) and the heat capacity C_V calculated for the Ni_{147} cluster, respectively. The heat capacity at constant volume is defined as a derivative of the internal energy over the temperature: $C_V = (\partial E/\partial T)_V$.

A thermal phase transition is indicated in the caloric curve by a change in the gradient of the temperature-dependent total energy $\langle E_{tot} \rangle$. The height of the jump near the phase transition point gives an estimate of the latent heat, *i.e.* the energy which is associated with the destruction of the ordered lattice. Figure 2 demonstrates that the change in the slope of the caloric curve takes place in the wide interval of temperatures between $T_{freezing}$ $\approx$ 600 K and $T_{melting} \approx$ 800 K. For the temperatures $T < T_{freezing}$, the cluster is completely frozen; while for temperatures $T > T_{melting}$, the cluster has melted. The intermediate interval $T_{freezing} < T < T_{melting}$ corresponds to the mixed state where the solid and the liquid phases coexist. This is a typical behavior of the caloric curve for finite systems, in contrast to the abrupt stepwise jump of the caloric curve corresponding to the melting temperature of a bulk.

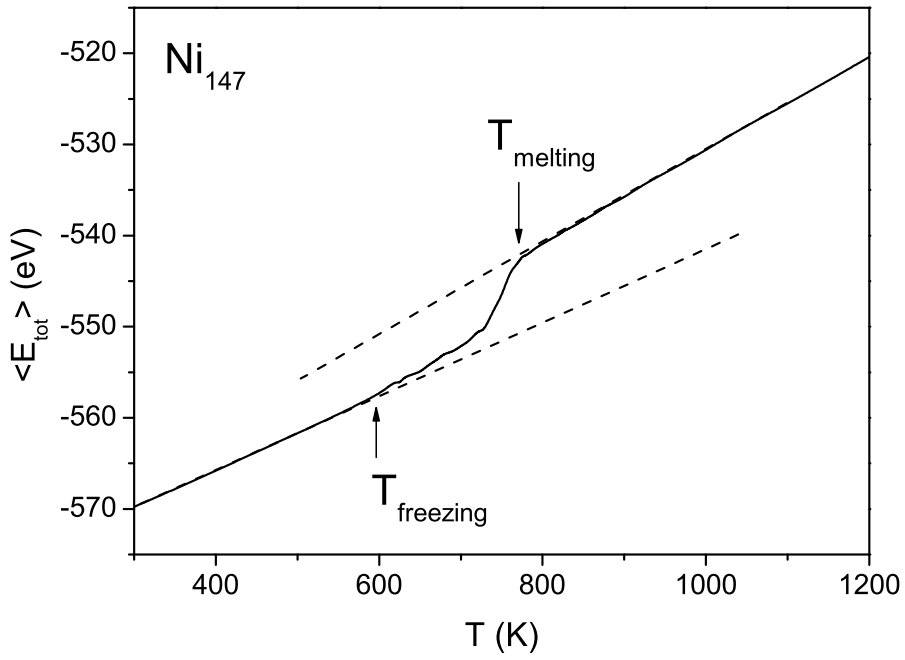

FIG. 2: Caloric curve for the pure Ni_{147} cluster. Temperatures $T < T_{freezing}$ and $T > T_{melting}$ correspond to the completely frozen and melted states, respectively.

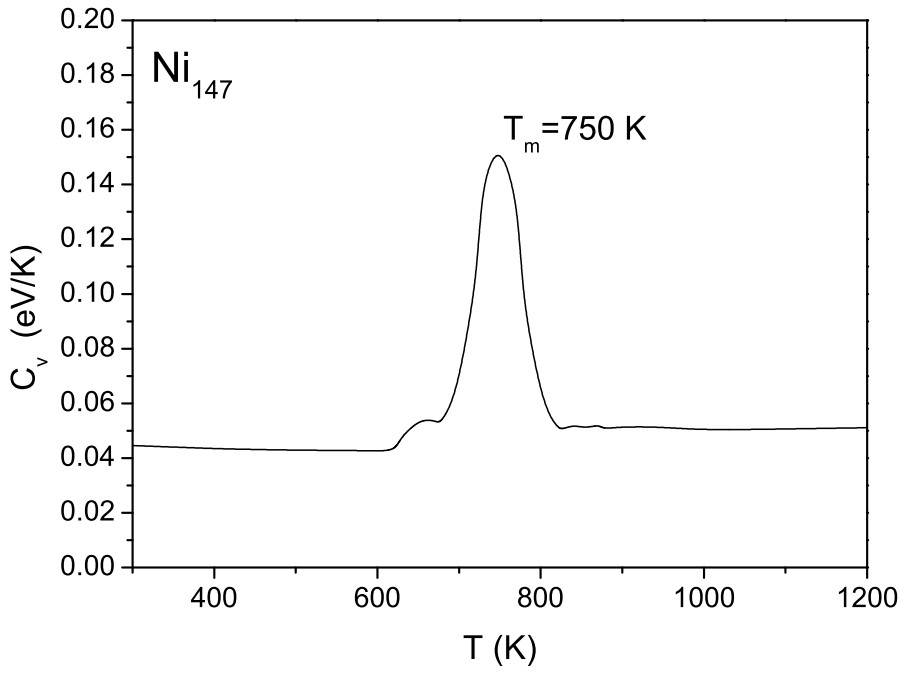

FIG. 3: Heat capacity for the pure Ni_{147} cluster as a function of T. Temperature $T_m = 750$ K indicates the melting temperature of the cluster (defined as the maximum of the heat capacity).

The melting process can also be easily recognized by the peak in the temperature dependence of the heat capacity, as seen in Fig. 3. We have found that for the pure Ni_{147} cluster the melting temperature associated with the maximum of the heat capacity $T_m = 750$ K is considerably smaller than the melting temperature for the bulk nickel $T_m^{bulk} = 1728$ K.[70] As was discussed above, the decrease in the melting temperature of the finite size clusters in comparison with the bulk occurs due to a substantial increase in the relative number of weakly bounded atoms on the cluster surface. According to the so-called 'Pawlow law' the melting temperature of a spherical particle possessing a homogeneous surface decreases linearly with increasing its inverse radius:[2]

$$T_m = T_m^{bulk}\left(1 - \frac{\alpha}{R}\right), \tag{4}$$

where R is the radius of the spherical particle and α is a constant, which can be defined by fitting the temperature T_m to available experimental data. Equation (4) is valid for the relatively large particles when shell effects are not important. The similar reduction in the melting temperature of the large Ni_N clusters with the number of atoms N ranging from 336 to 8007 has been reported in Ref. 5. Based on the calculated melting temperatures from Ref. 5, we have estimated the values of T_m^{bulk} and α to be 1590 K and 3.65 Å respectively. The radius of the cluster has been defined as $R = r_s N^{1/3}$, where $r_s = 1.375$ Å is the Wigner-Seitz radius for bulk nickel.[71]

Apart from the main peak, the heat capacity displays an additional maximum at $T \approx 660$ K—suggesting a stepwise melting process. This additional maximum corresponds to a slight change in the slope of the caloric curve beginning at $T_{freezing} \approx 600$ K. Such a situation corresponds to the so-called *pre-melted* state—when the cluster surface melts first while the core of the cluster remains frozen. This is the stationary state where the coexistence of two phases—liquid surface and frozen cluster core—is observed. The exact delimitation of the two phases is relative but can be defined from the difference in mobility of atoms taken from the cluster surface and its core. Visualization of the molecular dynamics trajectories of atoms located at the surface and in the core of the cluster confirms this interpretation.

Figures 4(a), 4(b), and 4(c) present the time dependence of the instantaneous values of the total energy calculated for the Ni_{147} cluster at the temperatures 600 K, 750 K, and 800 K, respectively. The total simulation time is 10 ns.

It is seen from Fig. 4(a) that the instantaneous values of the total energy oscillate around

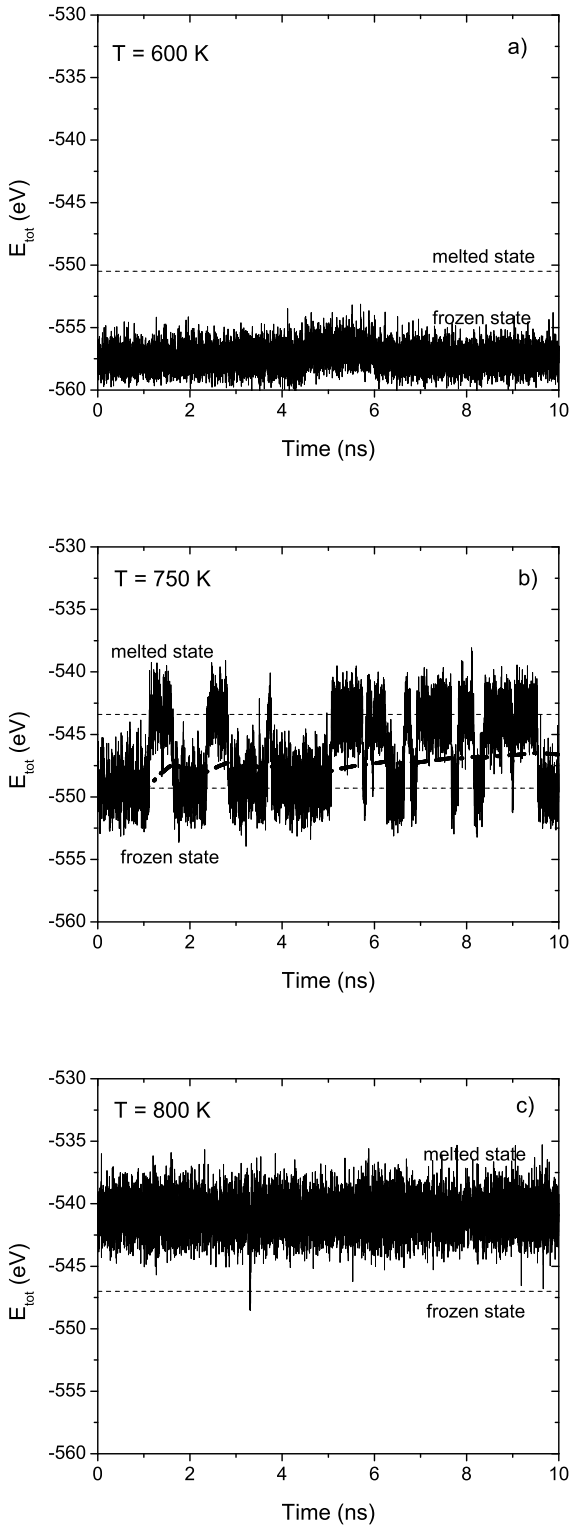

FIG. 4: Time dependence of the instantaneous values of the total energy calculated for the Ni_{147} cluster: (a) T = 600 K, frozen state; (b) T = 750 K, phase transition; (c) T = 800 K, molten state. The dashed-dotted lines demonstrate the time-averaged total energy of the system.

their time-averaged value at the cluster temperature $T = 600$ K. The fluctuations in the total energy of the system is a result of choosing the canonical ensemble of particles. To reproduce this ensemble, the temperature of the system is controlled by the Nosé-Hoover thermostat, which produces the appropriate energy fluctuations.[63,64] The frozen phase is characterized by thermal vibrations of the atoms around equilibrium positions in the cluster lattice, while the overall cluster structure remains unchanged.

For the temperature $T = 750$ K, corresponding to the maximum of the heat capacity, the time dependence of the instantaneous values of the total energy changes, as shown in Fig. 4(b). The total energy of the system initially oscillates around its typical averaged value for the frozen Ni_{147} state. After some time, the system jumps to a disordered molten state—causing the total energy of the system to oscillate around the average value typical for the molten Ni_{147} state. The system then, after a finite period in the molten state, jumps back to its initial frozen state. This behavior is repeated and the system continously oscillated between the frozen-molten states. Note that, in the interval of temperatures $T_{freezing} < T < T_{melting}$, it is necessary to perform the molecular dynamics simulations for a relatively long time (on the order of 10 ns) to achieve time independence of the averaged total energy $\langle E_{tot} \rangle$ of the system. The average life-time of the system in the frozen and the molten states depends upon the temperature of the cluster, resulting in a smooth change of the $\langle E_{tot} \rangle$ from the frozen to the molten state as a function of temperature. Thus, Fig. 4(b) clearly demonstrates coexistance of the two thermodynamic phases of the finite system at the temperature of phase transition. A similar behavior of the time dependence of the short-time potential energy averages calculated for the Ar_{13} cluster at the temperature 33 K has been reported in Refs. 72,73.

Finally, for the temperature $T = 800$ K and above, the total energy of the Ni_{147} cluster oscillates around its typical averaged value for the molten state.

B. C-doped Ni_{147} clusters

We now focus our study on the thermodynamic properties of the C-doped Ni_{147} cluster. We consider a cluster with the C impurity in the vicinity of the cluster center as shown in Fig. 1(b).

Dashed-dotted lines in Figs. 5 and 6 demonstrate the temperature dependence of the

caloric curve and the heat capacity calculated for the C-doped Ni_{147} cluster. For the sake of comparison, we have plotted the same dependencies calculated for the pure Ni_{147} cluster in Figs. 5 and 6 by solid lines. As seen in Figs. 5 and 6, doping of the Ni_{147} cluster with a single C impurity reduces its melting temperature by 30 K. Thus, doping of a cluster consisting of more than a hundred of atoms by just one additional atom of impurity results in a considerable change of its melting temperature.

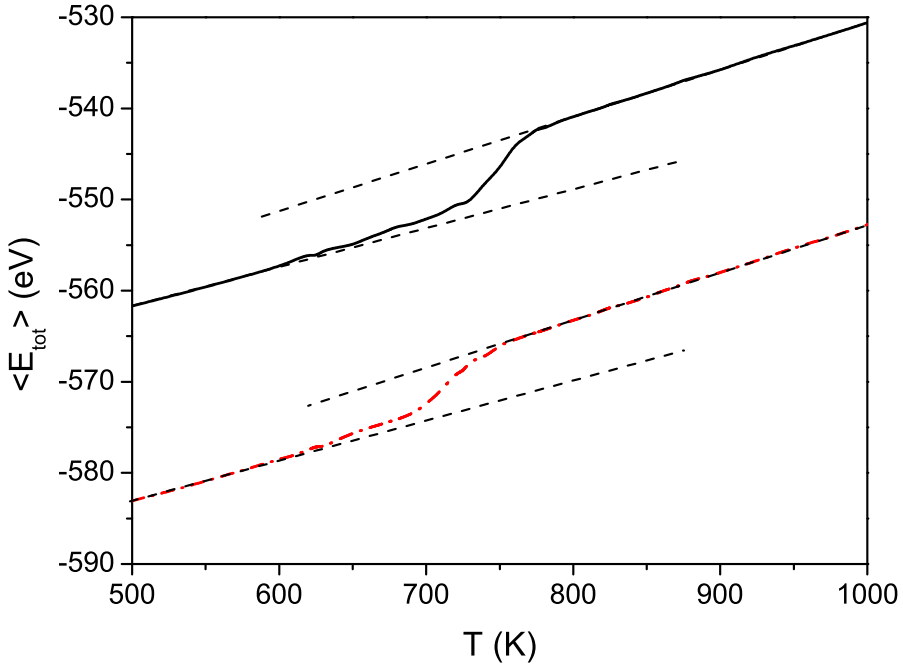

FIG. 5: Caloric curve for the pure Ni_{147} cluster (solid line) and the C-doped Ni_{147} cluster (dashed-dotted line).

Figure 5 demonstrates that the first change in the slope of the temperature-dependent $\langle E_{tot} \rangle$ calculated for the C-doped Ni_{147} cluster occurs at a temperature slightly below 600 K. This fact indicates that the C impurity does not have much influence on the surface melting of the cluster. Indeed, the C impurity is located near the cluster center where it induces local deformations. However, it does not significantly change the structure of the cluster surface, see Fig. 1(b); therefore, it does not have much of an effect on surface melting.

Further increase in the cluster temperature results in the melting of the C-doped Ni_{147} cluster with the melting temperature $T_m = 730$ K. The latter is defined by the position of the maximum of the temperature-dependent heat capacity. The decrease in the melting temperature of the C-doped Ni_{147} cluster can be explained as a result of the local distortions

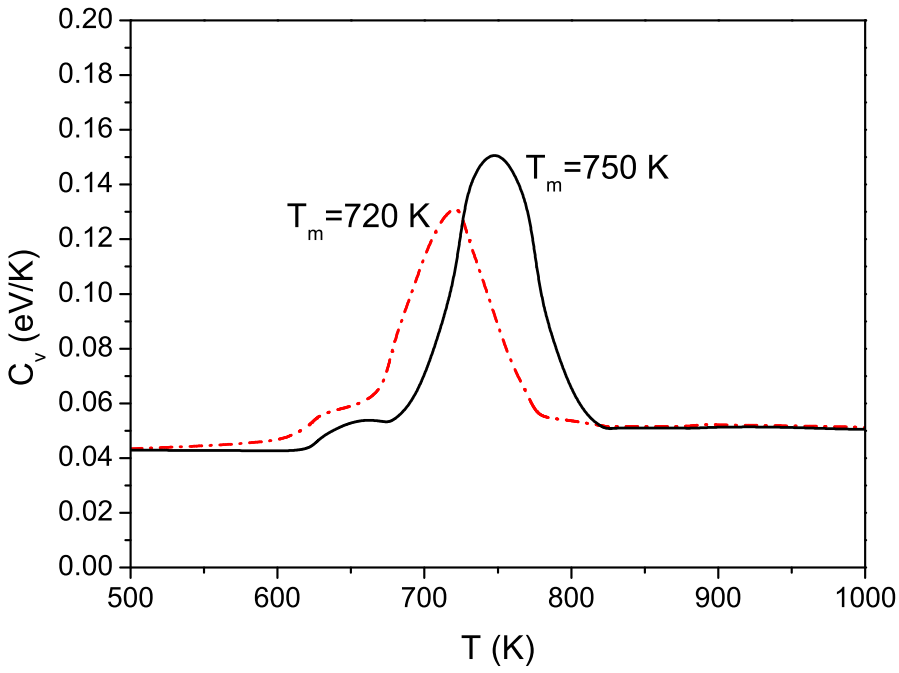

FIG. 6: Heat capacity for the pure Ni_{147} cluster (solid line) and the C-doped Ni_{147} cluster (dashed-dotted line) as a function of T. Temperatures $T_m = 750$ K and $T_m = 720$ K indicate the melting temperatures of the pure and the C-doped Ni_{147} cluster, respectively.

of the cluster's icosahedral structure near the impurity. The C atom introduces a strain in the cluster lattice which decreases stability of the cluster and thus, its melting temperature.

This effect is in accordance with the behavior of bulk material where it is known that defects in crystalline lattice provide nucleation sites for the liquid state (see, e.g., Ref. 59 and references therein). However such an effect strongly depends upon the type of impurity. As was demonstrated in Ref. 28, doping of the Ag_{55} cluster with Cu and Ni impurities in the center (where the bond length between Ag atoms and atoms of impurity are considerably smaller than the bond length between Ag atoms[28,59]) results in an increase of the melting temperature of the system. Therefore substitution of the central Ag atom with an atom of Cu or Ni impurity induces the contraction of the cluster lattice in the vicinity of the center, which can partially release the strain of the icosahedral structure.[28] Thus the small impurity in the center allows the cluster to relax toward a configuration with better interatomic distances, thereby increasing the cluster stability.[28,59]

Our results demonstrate that doping of the C atom in the vicinity of the center of the Ni_{147} cluster induces an additional strain in the cluster structure and, as a result, the melting

temperature of the cluster decreases. To study in detail how this induced strain can change the thermodynamic behavior of the C-doped Ni_{147} cluster, we have performed calculations of the melting temperature of the cluster for the set of different parameters ρ and r_0 in the Morse potential (3)—in other words, modeling the variation in the Ni – C interaction.

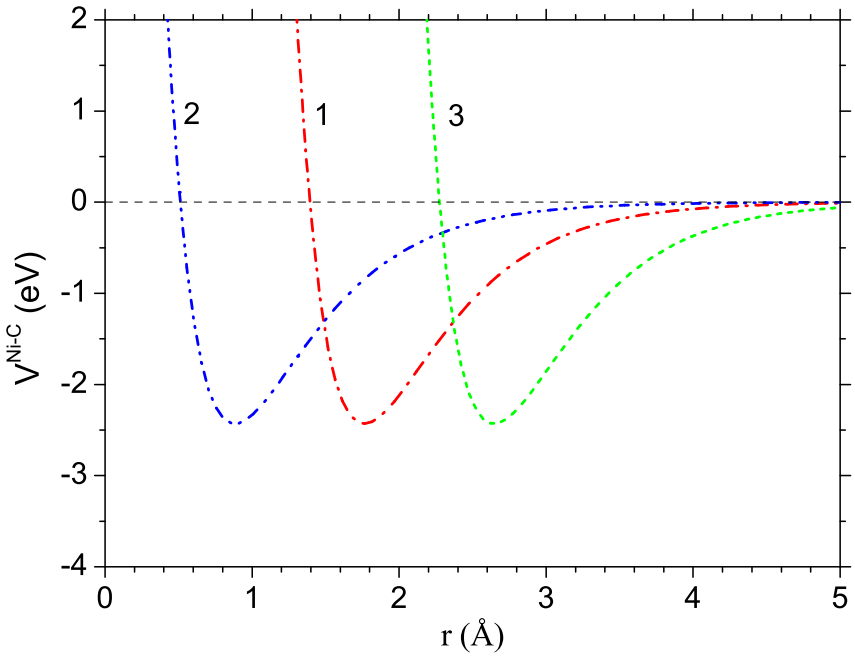

FIG. 7: (Color online) Morse potential for the Ni – C interaction with different values of parameters ρ and r_0. *Curve 1*, $\rho = 3.295$, $r_0 = 1.763$ Å (optimal values); *Curve 2*, $\rho = 1.648$, $r_0 = 0.882$ Å (reduced bonding); *Curve 3*, $\rho = 4.943$, $r_0 = 2.645$ Å (enlarged bonding). The depth of the potential well is kept constant $\varepsilon_M = 2.431$ eV.

Curve 1 in Fig. 7 presents the dependence of the Morse potential $V^{Ni-C}(r)$ on the interatomic distance r caclulated for the optimal values of the parameters ε_M, ρ, and r_0. Curve 2 in Fig. 7 presents the potential $V^{Ni-C}(r)$ when the bond constant r_0 and parameter ρ are reduced by the factor 0.5 in comparison to their optimal values; while curve 3 in Fig. 7 presents the interaction potential $V^{Ni-C}(r)$ when the parameters r_0 and ρ are enlarged by the factor 1.5. Hence, the potentials presented in Fig. 7 by curves 2 and 3 model the impurity effect with the local compression and expansion of the cluster lattice respectively.

To illustrate the effect of variation in the Ni – C interaction on cluster structure we present, in Figs. 8(a)-(c), the histogram of the radial distribution of the number of Ni atoms

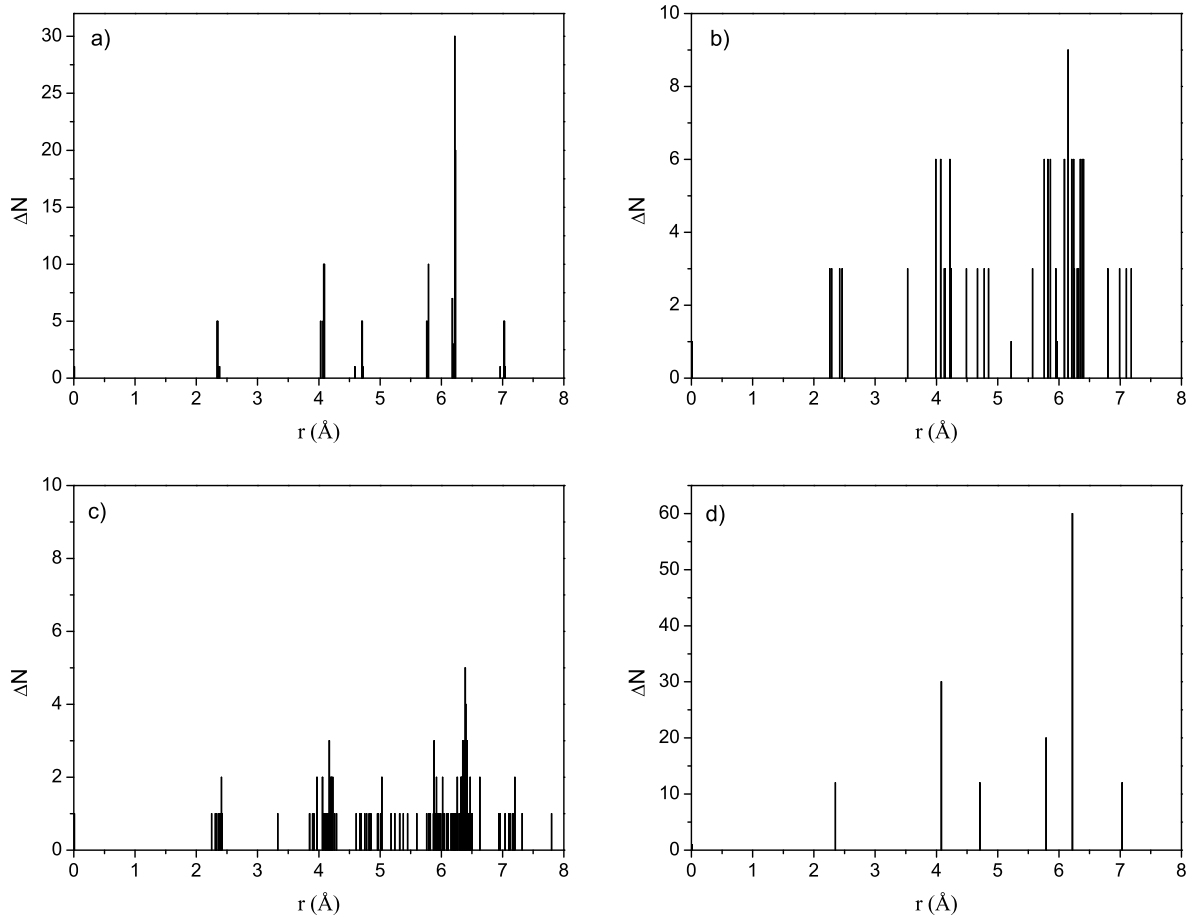

FIG. 8: The number of Ni atoms ΔN at distances between r and $r+\Delta r$ from the center of mass of the C-doped Ni_{147} cluster calculated for different values of the parameters ρ and r_0: (a) $\rho = 1.648$, $r_0 = 0.882$ Å (reduced bonding); (b) $\rho = 3.295$, $r_0 = 1.763$ Å (optimal values); (c) $\rho = 4.943$, $r_0 = 2.645$ Å (enlarged bonding); (d) pure Ni_{147} cluster for comparison. The radial interval Δr is 0.001 Å.

located at distances between r and $r + \Delta r$ from the center of mass of the C-doped Ni_{147} cluster (where the width of the radial interval is $\Delta r = 0.001$ Å). The change in the cluster structure, due to varying the parameters of ρ and r_0 in the Morse potential, can thus be clearly seen. For comparison, Fig. 8(d) represents the histogram of the radial distribution of the number of Ni atoms in the pure Ni_{147} cluster.

In the case of the reduced bonding between the C impurity and the Ni atoms, the overall icosahedral shell structure of the cluster remains preserved—although there exists some relaxation of the lattice, Fig. 8(a). The increase of the effective radius of the Morse potential

for the Ni – C interaction results in strong distortions of the icosahedral shell structure of the cluster, Figs. 8(b) and 8(c). Such distortions reduce the stability of the cluster in comparison to the compact icosahedral structure.

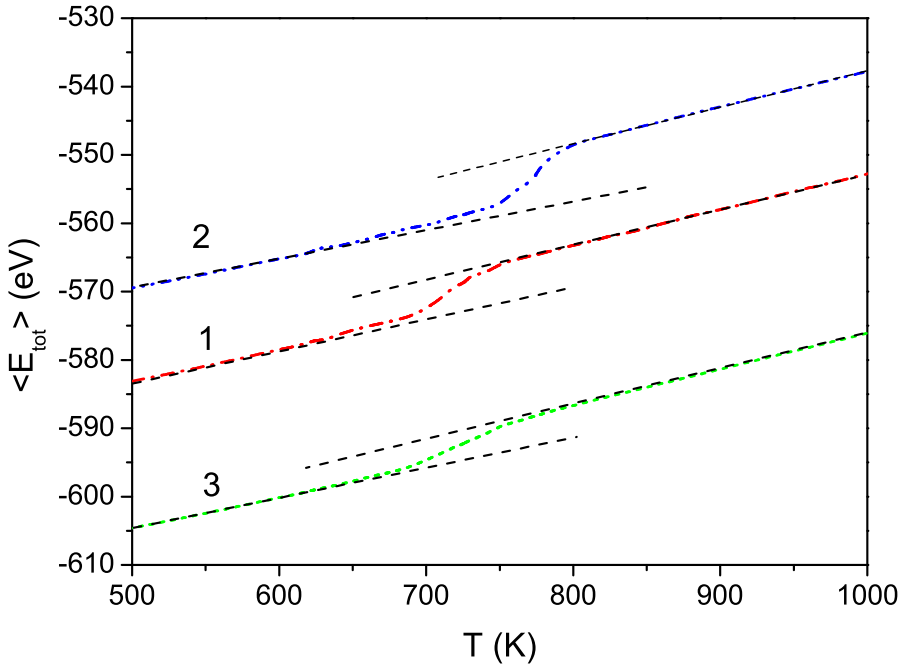

FIG. 9: (Color online) Caloric curves for the C-doped Ni_{147} cluster calculated for the different values of parameters ρ and r_0. *Curve 1*, $\rho = 3.295$, $r_0 = 1.763$ Å (optimal values); *Curve 2*, $\rho = 1.648$, $r_0 = 0.882$ Å (reduced bonding); *Curve 3*, $\rho = 4.943$, $r_0 = 2.645$ Å (enlarged bonding). The depth of the potential well is kept constant $\varepsilon_M = 2.431$ eV.

Figures 9 and 10 demonstrate the temperature dependence of the caloric curve and the heat capacity of the C-doped Ni_{147} cluster calculated for the different parameters of the Morse potential $V^{Ni-C}(r)$. Curves 1 in Figs. 9 and 10 present the caloric curve and the heat capacity calculated with the optimal values of parameters for the Ni – C interaction.

Decreasing the effective radius of the Morse potential (see curve 2, Fig. 7) by a factor 0.5 (*c.f.* the optimal values) results in the contraction of the cluster lattice in the vicinity of impurity. This contraction releases the strain in the icosahedral structure, therefore leading to an increase of the cluster stability. In this case the, melting temperature of the impurity doped Ni_{147} cluster increases by 21 K, compared the pure cluster (see curve 2 in Fig. 10).

An increase in the effective radius of the Morse potential for Ni – C interaction to its

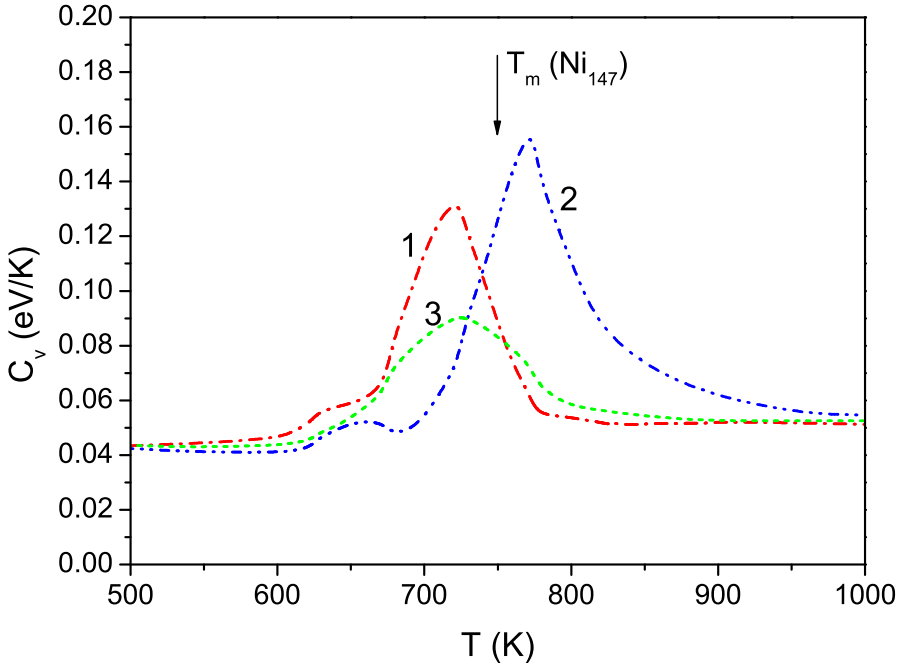

FIG. 10: (Color online) Heat capacity for the C-doped Ni_{147} cluster calculated for the different values of parameters ρ and r_0. *Curve 1*, $\rho = 3.295$, $r_0 = 1.763$ Å (optimal values); *Curve 2*, $\rho = 1.648$, $r_0 = 0.882$ Å (reduced bonding); *Curve 3*, $\rho = 4.943$, $r_0 = 2.645$ Å (enlarged bonding). The depth of the potential well is kept constant $\varepsilon_M = 2.431$ eV. Arrow indicates the melting temperature of the pure Ni_{147} cluster.

optimal value (see curve 1 in Fig. 7) results in the appearance of an additional strain in the cluster lattice. Therefore, the melting temperature of the C-doped Ni_{147} cluster decreases compared to the pure Ni_{147} cluster.

The further increase in the effective radius of the Ni – C interaction creates a strong deformation and rearrangement in the cluster structure, see Fig. 8(c). In this case, location of the impurity in the vicinity of the cluster center becomes energetically unfavorable. Thus, the impurity atom shifts towards the cluster surface to minimize the destruction of the icosahedral lattice. This effect prevents the further decrease in the melting temperature of the cluster, as an impurity located on the cluster surface will not have much influence on the melting transition of the core.

Melting transition can be also recognized from the analysis of the trajectories of the individual atoms and their diffusion in the volume of the cluster. The melting transition

occurs when atoms begin their Brownian motion instead of the thermal vibrations around their equilibrium positions in the ordered cluster's lattice. Such a transition can be seen as a step in the temperature dependence of the diffusion coefficient. The diffusion coefficient of the atom i in a media is defined as (see, e.g., Refs. 72,74):

$$D_i = \frac{1}{6}\frac{\mathrm{d}}{\mathrm{d}t}\left\langle r_i^2(t)\right\rangle, \tag{5}$$

where $\langle r_i^2(t)\rangle$ is the mean-square displacement averaged along the atom's trajectory

$$\left\langle r_i^2(t)\right\rangle = \frac{1}{n_t}\sum_{j=1}^{n_t}\left(\mathbf{R}_i(t_{0j}+t) - \mathbf{R}_i(t_{0j})\right)^2. \tag{6}$$

Here $\mathbf{R}_i(t)$ is a radius vector of an atom i at the time t, and n_t is the number of time origins, t_{0j}, considered along the trajectory. Equation (5) is valid for the simulation time smaller than the time required for a particle to migrate across the diameter of the cluster.

Figure 11 demonstrates the 2D projection of trajectories calculated for the Ni atom in the center of the C-doped Ni_{147} cluster (filled dots), the Ni atom from the vertex of the cluster surface (stars) and the C impurity (open dots). The temperature of the cluster ranges from 400 K to 800 K, as is shown in Fig. 11. The output time step is 1 ps with the total simulation time of 2 ns.

As seen in Fig. 11, for a low temperature, T = 400 K, all selected atoms in the C-doped Ni_{147} cluster vibrate around their equilibrium positions. At this temperature, the cluster is frozen—as per the analysis of the caloric curve and the heat capacity calculated for the C-doped Ni_{147} cluster, see Figs. 5 and 6).

It has been discussed above that the temperature dependence of the heat capacity of the C-doped Ni_{147} cluster exhibits two maxima corresponding to surface and volume melting of the cluster. It is seen from Fig. 6 that the first maximum in the temperature dependence of the heat capacity appears when the cluster is at T= 640 K (surface melting), while the second maximum appears at T= 720 K (volume melting). The temperature of 680 K corresponds to the intermediate state when the surface of the cluster has already melted but the cluster core is still frozen, as confirmed by the analysis of the atomic trajectories. As can be seen in Fig. 11 at T= 680 K, the surface Ni atom begins to diffuse on the surface, while the central Ni atom and the C impurity are still vibrating around their equilibrium positions. Note, that the icosahedral surface is inhomogeneous and consists of 12 vertices, 20 faces and 30

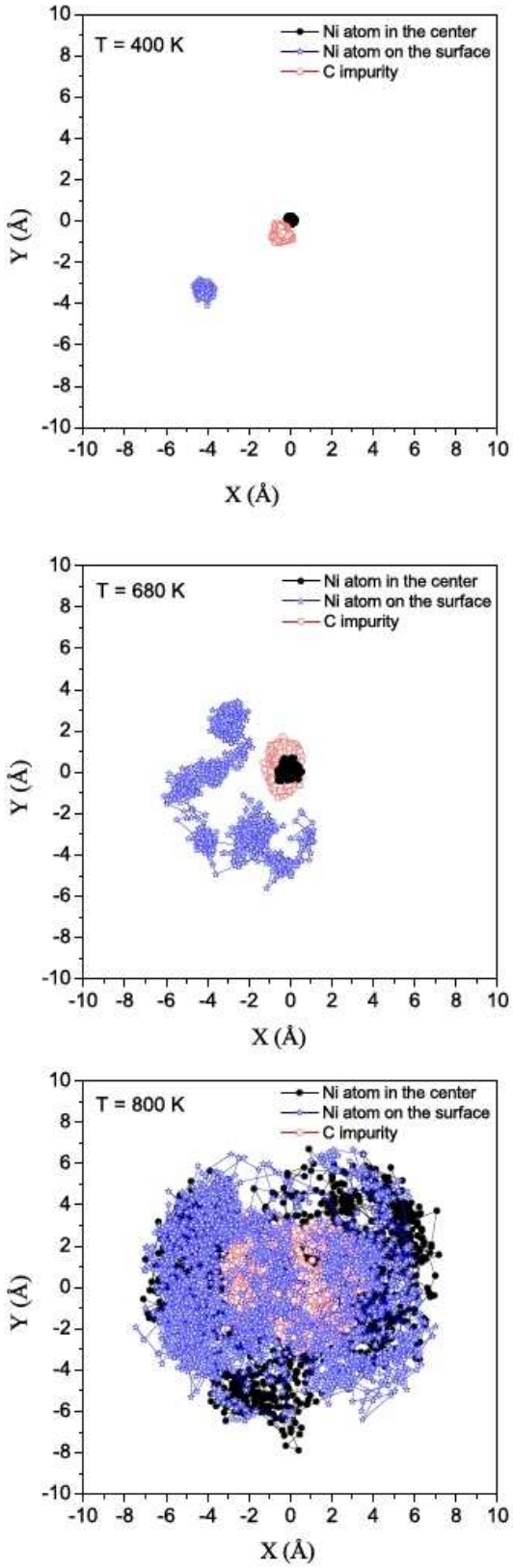

FIG. 11: (Color online) The 2D projection of trajectories calculated for the Ni atom in the center of the C-doped Ni_{147} cluster (filled dots), the Ni atom from the vertex of the cluster surface (stars) and the C impurity (open dots) for the cluster temperatures T = 400 K, 680 K, and 800 K. The output time step is 1 ps and the total simulation time is 2 ns.

edges. The binding energies of the atoms taken from the vertices, faces and edges are thus slightly different. Hence, these atoms begin diffusion at different temperatures.

Finally at the temperature of 800 K, cluster has completely melted as can be observed from the temperature behavior of the heat capacity presented in Fig. 6. Figure 11 demonstrates that the Ni atoms are moving in the entire volume of the cluster. The C impurity is also moving randomly in the cluster volume although the movement only occurs in the central part of the cluster. Hence, this supposes the heterogeneous distribution of the C atoms in the melted Ni_{147} clusters at T= 800 K.

The change in cluster structure upon melting is clearly seen in the time-averaged radial distribution of atoms in the cluster. The radial atomic distribution function $g(r)$ is defined as:

$$g(r) = dN(r)/dr, \tag{7}$$

where $dN(r)$ is the number of atoms in the spherical layer at distances between r and $r + dr$ from the center of mass of the cluster.

Figure 12 demonstrates the time-averaged radial distribution function $g(r)$ for Ni and C atoms in the C-doped Ni_{147} cluster calculated at cluster temperatures of $T = 300$ K, 600 K, 700 K, 720 K, 800 K, and 1000 K. The chosen range of temperatures allows for the analysis of the cluster structure in the frozen, transitional and molten states.

At the low cluster temperature, $T = 300$ K, one can see the icosahedral shell structure of of the nickel subsystem of the C-doped Ni_{147} cluster, consisting of the central atom and three icosahedral shells. The second and third shells are split—corresponding to atoms in vertex (12 atoms per shell) and non-vertex positions. Heating the cluster up to 600 K washes out the subshell splitting, nonetheless the icosahedral shells remain well separated.

With increase in the cluster temperature, up to 700 K, the second and the third shells beging to merge, although the first and the second shells are still separated (i.e., the radial distribution function $g(r)$ is equal to zero in the space between shells). At the temperature corresponding to the maximum in the heat capacity of the C-doped Ni_{147} cluster, $T = 720$ K, the first and second icosahedral shells merge.

Finally, at the temperatures corresponding to the molten state (800 K and 1000 K in Fig. 12), the distribution of Ni atoms become more homogeneous and the sharp shell structure washes out. Nevertheless, even at $T = 1000$ K, some radial order with maxima at 2.6 Å , 4.6 Å , and 6.5 Å still remains, suggesting that even a molten cluster of a finite size

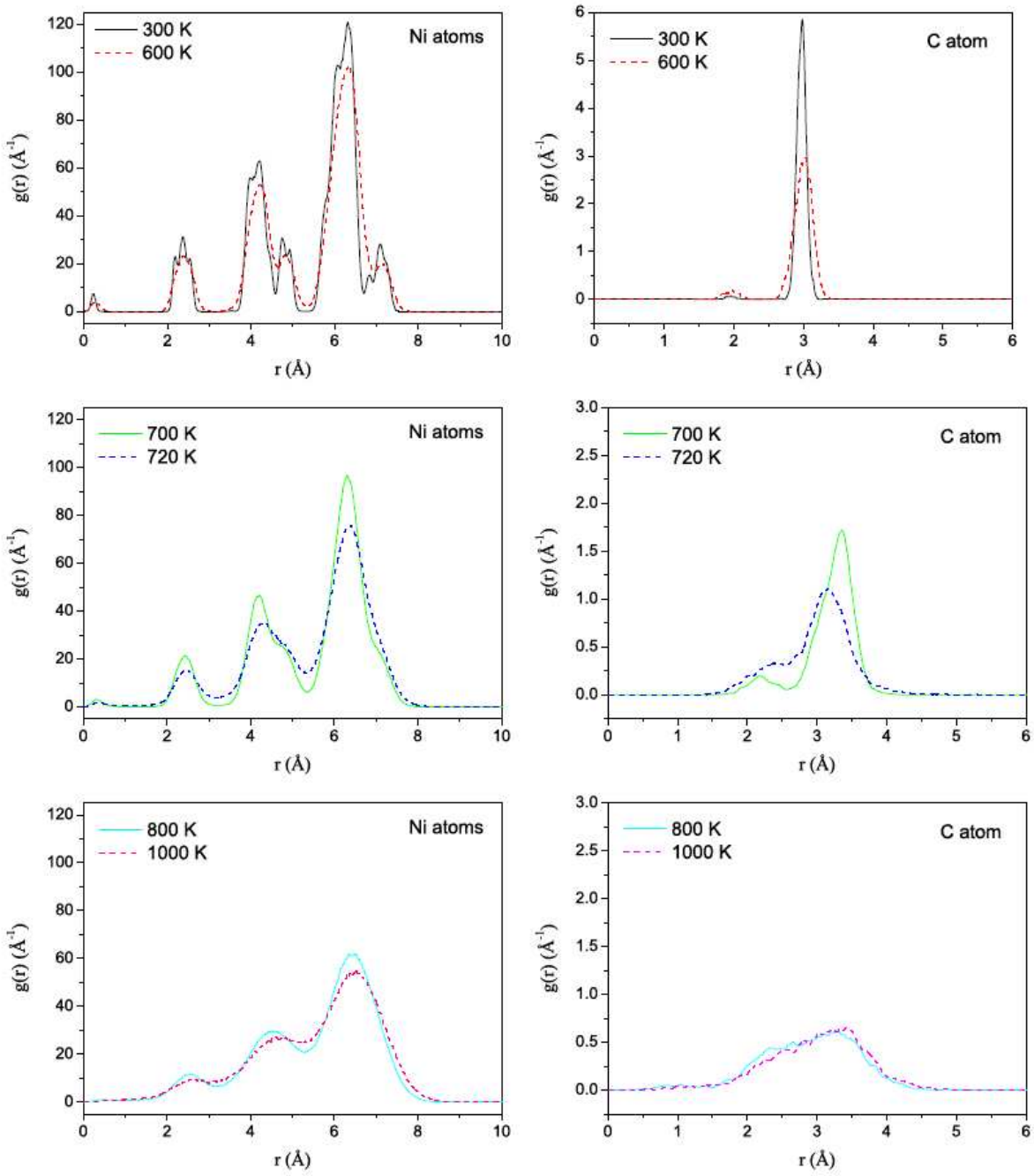

FIG. 12: (Color online) The time-averaged radial distribution function $g(r)$ calculated for the Ni and C atoms in the C-doped Ni_{147} cluster at different temperatures.

manifests some signs of a shell structure. This effect might be a general feature of finite systems, similar to the surface-induced ordering in liquid crystals or the layering effect at free liquid surfaces.[25,75,76]

Figure 12 demonstrates that, at cluster temperatures 300 K and 600 K, the time-averaged radial distribution function calculated for the C impurity atom exhibits a sharp maximum at distances 3 Å from the center of mass of the C-doped Ni_{147} cluster. Thus, at these temperatures, the C impurity is located between the first and the second icosahedral shells of the Ni atoms. By further increasing the cluster temperature to temperatures near the phase transition region, the radial distribution $g(r)$ of the C impurity becomes wider and the appearance of a second maximum at distances ≈ 2 Å can be observed. While at $T >$ 800 K, the C impurity can be found to be distributed in the central part of the cluster.

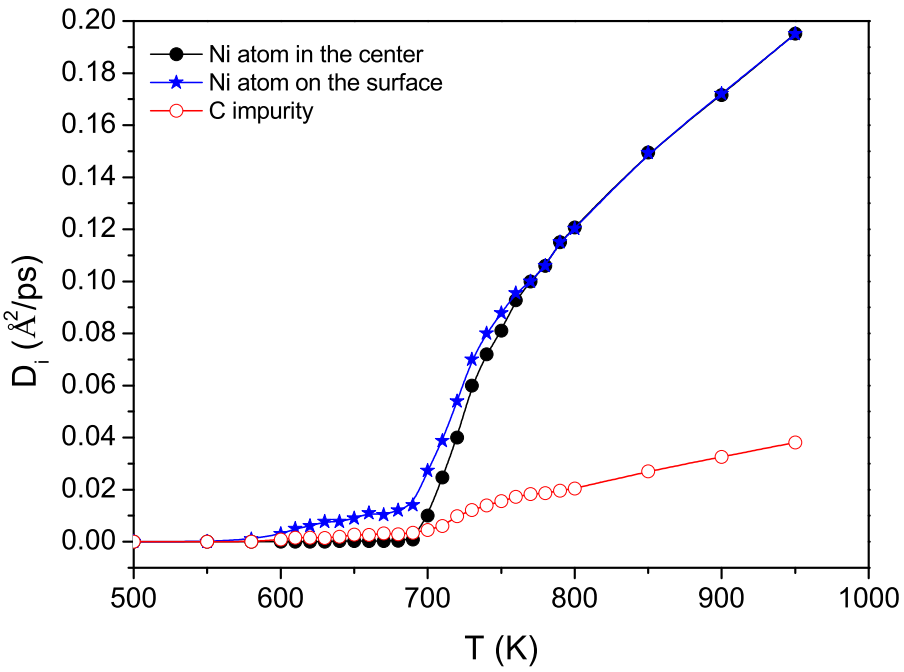

FIG. 13: (Color online) Temperature dependence of diffusion coefficients calculated for the Ni atom in the center of the C-doped Ni_{147} cluster (filled dots), the Ni atom on the cluster surface (stars) and the C impurity (open dots).

Figure 13 demonstrates the temperature dependence of diffusion coefficients calculated for the selected atoms in the C-doped Ni_{147} cluster. It is seen from Fig. 13 that the Ni atom on the cluster surface begins to diffuse at temperature of 600 K, while Ni atom in the cluster center and the C impurity remain frozen.

As has been shown above, the caloric curve calculated for the C-doped Ni_{147} cluster (see Fig. 5) clearly demonstrates a stepwise melting behavior. In the temperature interval $600 < T < 700$ K, the slope of the caloric curve changes slightly in comparison with that for the frozen state, suggesting the existence of a pre-melted state. For the temperatures $700 < T < 760$ the time-averaged total energy $\langle E_{tot} \rangle$ growing rapidly and finally reaches its asymptotic behavior at $T > 760$ K. The variations in the slope of the caloric curve result in the appearance of the two maxima in the temperature dependence of the heat capacity. These maxima are associated with the surface and core (volume) melting of the C-doped Ni_{147} cluster. This proposition is fully confirmed by the analysis of the temperature dependence of the diffusion coefficients for the Ni atoms from: a) the cluster surface and b) the cluster center.

Thus, in the temperature interval of $600 < T < 700$ K, only surface atoms diffuse, confirming that the initial melting of the cluster surface. The Ni atom located in the cluster center then begins to diffuse at T= 700 K. The diffusion coefficients calculated for Ni atoms located on the cluster surface and in the core are different up to $T = 760$ K. The difference in the diffusion coefficients show that the surface and the core atoms are not yet fully mixed in the cluster volume. The difference disappears at cluster temperatures of $T > 760$ K, when the C-doped Ni_{147} cluster has become completely molten.

Figure 13 demonstrates that the C impurity begins to diffuse at $T \approx 700$ K—similar to the central Ni atom. However, values of the diffusion coefficients calculated for the C impurity are considerably lower than those for the Ni atoms. Knowledge of the diffusion coefficients of the C impurity in a nickel cluster can be used for building a reliable kinetic model of carbon nanotube growth.[32,34]

IV. CONCLUSION

Doping of Ni_{147} with a carbon impurity lowers its melting temperature by 30 K due to excessive stress on the cluster lattice. The magnitude of the change induced is dependent upon the parameters of the interaction between the nickel atoms and the carbon impurity. We have demonstrated that an induced contraction of the icosahedral cluster's lattice in the vicinity of the impurity results in an increase of the melting temperature of the cluster; whereas additional strain in the lattice results in the reduction of the melting tempera-

ture. Therefore, the melting temperature of atomic clusters can be effectively tuned by the addition of an impurity of a particular type.

Doping by a C impurity changes the melting temperature of the cluster, consequently this means that doping affects the mobility of the atoms in the Ni cluster. This effect has to be taken into consideration in particular applications with metal clusters when the entire process depends on the thermodynamic state of the cluster. An example of such experiment is the process of the catalytically activated growth of carbon nanotubes. The kinetics of the carbon nanotube growth depends upon diffusion of carbon atoms through the metal catalyst. Presence of the impurities can considerably change the flux, thereby affecting the growth rate of the carbon nanotube. The additional change in the thermodynamic state of the catalytic particle in the nanotube growth process might also depend on the strength of the interaction of the particle with a substrate.

In the present work, we have considered a single C impurity in the cluster of Ni_{147}. We intend to further study the effect of how several C impurities will influence the thermodynamic properties of the host cluster. In particular, it is important to find the optimum conditions (concentration of C atoms, temperature, thermodynamic state of the particle, etc.) when the C atoms begin aggregating into ordered carbon structures, such as nanotubes.

The influence of impurities on properties of finite systems is a general effect. While our results were obtained for free clusters, many interesting problems can be found when one considers the influence of impurities on the phase transitions and stability of clusters deposited on a substrate. Thus, recently it has been experimentally shown that the oxidation of silver clusters deposited on a HOPG surface changes the stability and morphology of cluster formations.[77,78] Clusters on substrates have important technological applications and the understanding of how these clusters stabilize on the surface are of profound interest.

Acknowledgments

This work is partially supported by the European Commission within the PECU project (contract No. 4916 (NEST)) and Network of Excellence project EXCELL. The authors gratefully acknowledge support by the Frankfurt Center for Scientific Computing.

References

* On leave from Institute of Physics, St. Petersburg State University, Ulianovskaya Str. 1, 198504 St. Petersburg, Petrodvorez, Russia; Email address: lyalin@fias.uni-frankfurt.de

† On leave from A. F. Ioffe Physical-Technical Institute, Polytechnicheskaya 26, 194021 St. Petersburg, Russia

[1] W. Thomson, Philos. Mag. **42** 448 (1871)

[2] P. Pawlow, Z. Phys. Chem. **65**, 1 (1909)

[3] M. Takagi, J. Phys. Soc. Japan **9** 361 (1954)

[4] K.J. Hanszen, Z. Phys. Chem. **157** 523 (1960)

[5] Y. Qi, T. Çhağin, W.L. Johnson, W.A. Goddard III, J. Chem. Phys. **115** 385 (2001)

[6] Ph. Buffat and J.-P. Borel, Phys. Rev. A **13** 2287 (1976)

[7] T. Castro, R. Reifenberger, E. Choi, and R.P. Anders, Phys. Rev. B **42** 8548 (1990)

[8] S. Lai, J.Y. Guo, V. Petrova, G. Ramanath and L.H. Allen Phys. Rev. Lett. **77** 99 (1996)

[9] C. E. Bottani, A. Li Bassi, B. K. Tanner A. Stella, P. Tognini,P. Cheyssac, and R. Kofman, Phys. Rev. B **59** R15601 (1999)

[10] M. Schmidt, R. Kusche, W. Kronmüller, B. von Issendorff, and H. Haberland Phys. Rev. Lett. **79** 99 (1997)

[11] M. Schmidt, R. Kusche, B. von Issendorff, and H. Haberland Nature **393**, 238 (1998)

[12] R. Kusche, Th. Hippler, M. Schmidt, B. von Issendorff, and H. Haberland Eur. Phys. J. D **1** 9 (1999)

[13] H. Haberland, Th. Hippler, J. Donges, O. Kostko, M. Schmidt, and B. von Issendorff Phys. Rev. Lett. **94** 035701 (2005)

[14] F. Calvo, F. Spiegelmann, J. Chem. Phys. **112** 2888 (2000)

[15] J.A. Reyes-Nava, I.L. Garzon, K. Michaelian, Phys. Rev. B **67**, 165401 (2003)

[16] F. Calvo, F. Spiegelmann, J. Chem. Phys. **120** 9684 (2004)

[17] K. Manninen, A. Rytkonen, M. Manninen, Eur. Phys. J. D **29**, 39 (2004)

[18] S. Chacko, D.G. Kanhere, S.A. Blundell, Phys. Rev. B **71**, 155407 (2005)

[19] A. Aguado, J.M. López, Phys. Rev. Lett. **94**, 233401 (2005)

[20] A. Aguado, J. Phys. Chem. B **109**, 13043 (2005)

[21] E.G. Noya, J.P.K. Doye, D.J. Wales, and A. Aguado, Eur. Phys. J. D **43**, 57 (2007)

[22] A.A. Shvartsburg and M.F. Jarrold, Phys. Rev. Lett. **85**, 2530 (2000)

[23] G.A. Breaux, R.C. Benirschke, T.Sugai, B.S. Kinnear, and M.F. Jarrold, Phys. Rev. Lett. **91**, 215508 (2003)

[24] S. Darby, T.V. Mortimer-Jones, R.L Johnston, C.J. Roberts, Chem. Phys., **116**, 1536 (2002)

[25] A. Aguado, L.E. González, and J.M. López, J. Phys. Chem. B **108**, 11722 (2004)

[26] P. Chandrachud, K. Joshi, and D. G. Kanhere, Phys. Rev. B **76**, 235423 (2007)

[27] C. Hock, S. Strassburg, H. Haberland, B. v. Issendorff, A. Aguado, and M. Schmidt Phys. Rev. Lett. **101**, 023401 (2008)

[28] C. Mottet. G.Rossi, F. Baletto, and R. Ferrando, Phys. Rev. Lett. **95**, 035501 (2005)

[29] W. A. Goddard III, D.W. Brenner, S. Lyshevski, and G. Iafrate (eds.), Handbook of Nanoscience, Engineering, and Technology, CRC Press (2007)

[30] V. B. Golovko, H. W. Li, B. Kleinsorge, S. Hofmann, J. Geng, M. Cantoro, Z. Yang, D. A. Jefferson, B.F.G. Johnson, W.T.S. Huck, and J. Robertson, Nanotechnology, **16** 1636 (2005)

[31] O. I. Obolensky, I. A. Solov'yov, A. V. Solov'yov, and W. Greiner, Book of Abstracts, p. 132, Symposium on Size Selected Clusters (S3C), Brand, Austria, March 12 - 16, 2007.

[32] O. I. Obolensky, I. A. Solov'yov, A. V. Solov'yov, and W. Greiner, Abstracts of the International Symposium "Atomic Cluster Collisions: structure and dynamics from the nuclear to the biological scale" (ISACC 2007), ed. A.V. Solov'yov, europhysics conference abstracts, p. 176, vol. 31D (European Physical Society, 2007)

[33] A.R. Harutyunyan, T. Tokune, and E. Mora, Appl. Phys. Lett. **87**, 051919 (2005)

[34] O.A. Louchev, Th. Laude, Y. Sato, and H. Kanda, J. Chem. Phys. **118**, 7622 (2003)

[35] R.T.K. Baker and P.S. Harris in *Chemistry and Physics of Carbon*, eds. P.L. Walker, Jr. and P.A. Thrower (Dekker, New York, 1978)

[36] S. Nayak, S.N. Khanna, B.K. Rao, and P. Jena, J. Phys. Chem. A **101**, 1072 (1997)

[37] A.P. Sutton, J. Chen, Philos. Mag. Lett. **61**, 139 (1990)

[38] M.S. Daw, M.I. Baskes, Phys. Rev. Lett. **50**, 1285 (1983)

[39] M.S. Daw, M.I. Baskes, Phys. Rev. B **29**, 6443 (1984)

[40] S.M. Foiles, M.S. Daw, and M.I. Baskes, Phys. Rev. B **33**, 7983 (1986)

[41] M.W. Finnis, J.E. Sinclair, Philos. Mag. **50**, 45 (1984)

[42] A.P. Sutton, P.D. Godwin, and A.P. Horsfield, MRS Bull. **21**, 42 (1996)

[43] H. Raffi-Tabar, A.P. Sutton, Philos. Mag. Lett. **63**, 217 (1991)

[44] B.D. Todd, R.M. Lynden-Bell, Surf. Sci. **281**, 191 (1993)

[45] R.M. Lynden-Bell, J. Phys.: Condens. Matter. **7**, 4603 (1995)

[46] J.P.K. Doye, and D. Wales, New J. Chem. **22**, 733 (1998)

[47] Y. Yamaguchi, and S. Maruyama, Eur. Phys. J. D **9**, 385 (1999)

[48] Y. Shibuta, S. Maruyama, Comp. Mat. Sci. **39**, 842 (2007)

[49] A. Martinez-Limia, J. Zhao, and P. Balbuena, J. Mol. Model. **13**, 595 (2007)

[50] A. D. Becke, Phys. Rev. A **38**, 3098 (1988)

[51] A. D. Becke, J. Chem. Phys. **98**, 5648 (1993)

[52] C. Lee, W. Yang, and R. G. Parr, Phys. Rev. B **37**, 785 (1988)

[53] James B. Foresman and Æleen Frisch, *Exploring Chemistry with Electronic Structure Methods* (Gaussian Inc., Pittsburgh, PA, 1996).

[54] I.A.Solov'yov, A.V.Solov'yov, W.Greiner, A.Koshelev and A.Shutovich, *Phys. Rev. Lett.* **90**, 053401 (2003)

[55] I.A.Solov'yov, A.V.Solov'yov, W.Greiner, Int. J. Mod. Phys. E **13** 697 (2004)

[56] O. I. Obolensky, I. A. Solov'yov, A. V. Solov'yov, W. Greiner, Computing Letters (CoLe) **1**, 313 (2005)

[57] D.E. Goldberg, Genetic Algorithms in Search, Optimization, and Machine Learning. Addison-Wesley, Reading, MA, 1989.

[58] Z. Michalewicz, Genetic Algorithms + Data Structures = Evolution Programs. Springer, Berlin, Heidelberg, New York. (3rd Ed.), 1996.

[59] R. Ferrando, J. Jellinek, and R. L. Johnston, Chem. Rev. **108**, 845 (2008)

[60] A. Lyalin, I.A. Solov'yov, A.V. Solov'yov and W. Greiner, Phys. Rev. A **67**, 063203 (2003)

[61] A. Lyalin, A.V. Solov'yov, and W. Greiner, Phys. Rev. A **74**, 043201 (2006)

[62] A. Lyalin, I.A. Solov'yov, A.V. Solov'yov and W. Greiner, Phys. Rev. A **75**, 053201 (2007)

[63] S. Nose, J. Chem. Phys. **81**, 511 (1984)

[64] W.G. Hoover, Phys. Rev. A **31**, 1695 (1985)

[65] J.A. Alonso, *Structure and properties of atomic nanoclusters* (Imperial College Press, London 2005).

[66] F. Baletto and R. Ferrando, Rev. Mod. Phys. **77**, 371 (2005)

[67] M. Pellarin, B. Baguenard, J.L. Vialle, J. Lermé, M. Broyer, J. Miller and A. Perez, Chem. Phys. Lett. **217**, 349 (1994)

[68] J.M. Montejano-Carrizales, M.P. Iñiguez, J.A. Alonso, M.J. López, Phys. Rev. B 54, 5961 (1996)

[69] Z. Zhang, W. Hua, and S. Xiao, J. Chem. Phys. **122**, 214501 (2005)

[70] R. Canselow and R.F. Howe (eds.), Chemistry and physics of Solid Surfaces VII, (Springer, Heidelberg, 1988).

[71] C. Kittel, *Introduction to Solid State Physics*, 7th edn., (John Wiley and Sons, New York, 1996)

[72] J. Jellinek, T.L. Beck, and R.S. Berry, J. Chem. Phys. **84**, 2783 (1986)

[73] H. L. Davis, J. Jellinek, and R.S. Berry, J. Chem. Phys. **86**, 6456 (1987)

[74] L. D. Landau, E. M. Lifshitz, Course of Theoretical Physics, Vol. 6: Fluid Mechanics, 2nd Ed., Pergamon Press, (1987)

[75] B. M. Ocko, A. Braslau, P. S. Pershan, J. Als-Nielsen, and M. Deutsch Phys. Rev. Lett. **57**, 94 (1986)

[76] E. Chacón, M. Reinaldo-Falagán, E. Velasco and P. Tarazona Phys. Rev. Lett. **87**, 166101 (2001)

[77] A. Lando, N. Kébaïli, Ph. Cahuzac, A. Masson, C. Bréchignac, Phys. Rev. Lett. **97**, 133402 (2006)

[78] A. Lando, N. Kébaïli, Ph. Cahuzac, C. Colliex, M. Couillard, A. Masson, M. Schmidt, and C. Bréchignac, Eur. Phys. J. D **43**, 151 (2007)